



## Constraining a land surface model with multiple observations by application of the MPI-Carbon Cycle Data Assimilation System

G. J. Schürmann<sup>a</sup>, T. Kaminski<sup>b,d</sup>, C. Köstler<sup>a</sup>, N. Carvalhais<sup>a</sup>, M. Vößbeck<sup>b,d</sup>, J. Kattge<sup>a</sup>, R. Giering<sup>c</sup>, C. Rödenbeck<sup>a</sup>, M. Heimann<sup>a</sup>, and S. Zaehle<sup>a</sup>

<sup>a</sup>Max Planck Institute for Biogeochemistry, Hans-Knöll-Str. 10, 07745, Jena, Germany

<sup>b</sup>The Inversion Lab, Hamburg

<sup>c</sup>FastOpt, Hamburg

<sup>d</sup>previously at FastOpt, Hamburg

Correspondence to: G. Schürmann (gschuer@bgc-jena.mpg.de) and S. Zaehle (soenke.zaehle@bgc-jena.mpg.de)

**Abstract.** We describe the Max Planck Institute Carbon Cycle Data Assimilation System (MPI-CCDAS) built around the tangent-linear version of the land surface scheme of the MPI-Earth System Model v1 (JSBACH). The simulated terrestrial biosphere processes (phenology and carbon balance) were constrained by observations of the fraction of photosynthetically active radiation (TIP-FAPAR product) and by observations of atmospheric CO<sub>2</sub> at a global set of monitoring stations for the years 2005 - 2009. The system successfully, and computationally efficiently, improved average foliar area and northern extra-tropical seasonality of foliar area when constrained by TIP-FAPAR. Global net and gross carbon fluxes were improved when constrained by atmospheric CO<sub>2</sub>, although the system tended to underestimate tropical productivity. Assimilating both data streams jointly allowed the MPI-CCDAS to match both observations (TIP-FAPAR and atmospheric CO<sub>2</sub>) equally well as the single data stream assimilation cases, therefore overall increasing the appropriateness of the resultant parameter values and biosphere dynamics. Our study thus highlights the role of the TIP-FAPAR product in stabilising the underdetermined atmospheric inversion problem and demonstrates the value of multiple-data stream assimilation for the simulation of terrestrial biosphere dynamics. The constraint on regional gross and net CO<sub>2</sub> flux patterns is limited through the parametrisation of the biosphere model. We expect improvement on that aspect through a refined initialisation strategy and inclusion of further biosphere observations as constraints.

but that's what you assimilated.

### 1 Introduction

Estimates of the net carbon balance of the terrestrial biosphere are highly uncertain (Le Quéré et al., 2015), because the net balance cannot be directly observed at large spatial scales. Studies aiming to quantify the contemporary global carbon cycle therefore either infer the terrestrial carbon budget as a residual of the arguably better constrained other components of the global carbon budget (Le Quéré et al., 2015), or rely on measurements of atmospheric CO<sub>2</sub> and the inversion of its atmospheric transport (Gurney et al., 2002).

Both approaches have the caveat that they are not able to provide accurate estimates at high spatial resolution, and cannot utilise the broader set of Earth system observations that provide information on terrestrial carbon cycle dynamics (Luo et al., 2012). Further, they are diagnostic by nature, and lack therefore any prognostic capacity.

Ecosystem models integrate existing knowledge of the underlying processes governing the net terrestrial carbon balance and have such a prognostic capacity. Since they simulate all major aspects of the terrestrial carbon cycle, they can - in principle - benefit from the broader set of Earth system observations. However, studies comparing different land surface models show a large spread of estimates of the seasonal and annual net land-atmosphere carbon exchange and their trends (Piao et al., 2013; Sitch et al., 2015). This uncertainty is one of the primary causes for discrepancies in future projections of stand-alone terrestrial biosphere models (Sitch et al., 2008), and coupled carbon cycle climate model projections (Anav et al., 2013; Friedlingstein et al., 2014) for the 21st century. Next to the uncertainty due to different climate forcing (Jung et al., 2007; Dalmonech et al., 2015) and alter-



native model formulations (Sitch et al., 2015), the uncertainty about the parameter values of the mathematical representation of key carbon cycle processes in these models are an important source of the model spread (Knorr and Heimann, 2001; Zachle et al., 2005; Booth et al., 2012). This parametric uncertainty can be as large as the differences between models. The spread among models limits our ability to provide further constraints of the net terrestrial carbon uptake.

A potential route to reduce parameter and process-formulation related uncertainties in the estimates of the terrestrial carbon cycle is to systematically integrate the increasing wealth of globally distributed carbon cycle observations into models through data assimilation methods. A broad overview of potential observations and methodological choices is given in Raupach et al. (2005). A prototype of such a carbon cycle data assimilation system (CCDAS) based on an advanced variational data assimilation scheme and a prognostic terrestrial carbon flux model (BETHY; Knorr 1997, 2000) has demonstrated the potential to effectively constrain the simulated carbon cycle with observations of atmospheric CO<sub>2</sub> (Rayner et al., 2005; Scholze et al., 2007; Kaminski et al., 2013). Conceptually similar systems have been built for other global biosphere models. For example, Luke (2011) constrained the phenology of the JULES model and Kuppel et al. (2012, 2013) applied the ORCHIDEE model at a series of FLUXNET-sites to estimate process parameters across these sites and further demonstrated the usefulness of the approach to improve globally modelled CO<sub>2</sub>. Whereas the above systems rely on precise calculation of the gradients by a tangent-linear or adjoint version of the biosphere model, another CCDAS-like work demonstrated the assimilation of several data streams with the VISIT-model, approximating the gradient with finite differences (Saito et al., 2014). Knorr and Kattge (2005) investigated the use of a Monte-Carlo approach for data assimilation with global models and suggested that the computational burden (run time) is too large to allow its use with a comprehensive land surface model and a reasonable parameter vector. Ziehn et al. (2012) managed to apply a Monte Carlo algorithm to a global set-up of BETHY with a reduced parameter vector.

To make progress in the representation of carbon cycle dynamics in one process-based land surface model included in a coupled carbon cycle climate model, we have developed a CCDAS system for the JSBACH land surface scheme (Radatz et al., 2007) of the MPI-Earth System Model (MPI-ESM; Giorgetta et al., 2013). JSBACH is a further development of the BETHY model, providing a more detailed treatment of carbon turnover and storage in the terrestrial biosphere, as well as more detailed treatment of land surface biophysics (Roeckner et al., 2003) and land hydrology (Hagemann and Stacke, 2014). Here we present the development and first application of a variational data assimilation system built around the JSBACH model (Max Planck Institute Carbon Cycle Data Assimilation System: MPI-CCDAS). Our objective with this development is twofold: i) to improve

the scope of the original CCDAS by including a larger set of terrestrial processes affecting the terrestrial carbon cycle; and ii) to provide a means to constrain the land carbon cycle projections of JSBACH, and in hindsight also that of the MPI-ESM. While the MPI-CCDAS is driven with observed meteorology, and differences in the simulated terrestrial carbon cycle between JSBACH (with observed meteorology or coupled to the ESM exist (Dalmonech et al., 2015), certain features of the land processes are robust to the climate biases of the MPI-ESM, such that one might expect an improved carbon representation in the entire MPI-ESM after application of the MPI-CCDAS.

In this paper, we provide the technical description of the MPI-CCDAS system. We then demonstrate the capacity of the MPI-CCDAS system to simultaneously integrate atmospheric CO<sub>2</sub> observations and the fraction of absorbed photosynthetically active radiation (FAPAR) recorded from satellites, which constrains the seasonality of the phenology, and assesses the relative effect of the constraint from these two data streams on parameter values and modelled fluxes.

## 2 Description of MPI-CCDAS

### 2.1 CCDAS-Method

The MPI-CCDAS relies on a variational data assimilation approach to estimate a set of model parameters. In the following we give a brief overview of this method, and refer for a detailed description to Kaminski et al. (2013). To take account of the uncertainty inherent in the description of observed and simulated variables the method operates on probability density functions (PDFs). It is conveniently formulated in a Gaussian framework and uses the combined information provided by the model  $M(p)$  and the observations  $d$  to update a PDF that describes the prior state of information on the parameter vector  $p$  (more precisely on the control vector, which is a combination of the model's process parameters and of initial state variables). This prior control vector is described by the mean  $p_{pr}$  and the covariance of its uncertainty  $C_{pr}$ . The update of the prior PDF is called posterior PDF and its mean minimises the cost function  $J$ .

$$J(p) = \frac{1}{2} (M(p) - d)^T C_d^{-1} (M(p) - d) + (p - p_{pr})^T C_{pr}^{-1} (p - p_{pr}) \quad (1)$$

where  $C_d$  is the covariance of combined uncertainty in the observations (with mean  $d$ ) and model simulation. The minimum  $p_{po}$  of  $J$  (posterior control vector) thus balances the misfit between modelled quantities and their observational counterparts, while taking independent prior information on the control vector into account.

Technically,  $J$  is minimized through an iterative procedure using the Davidon-Fletcher-Powell algorithm in the

driven  
unclear

$\bar{p}_r$

not defined  
 $\bar{p}_o$



*is something missing here*

$\frac{\partial p}{\partial t}$  is evaluated by the tangent-linear version of the model which was generated via automatic differentiation (TAF: Giering and Kaminski 1998) of the model's source code.

## 2.2 The forward model

The model that is optimised within the MPI-CCDAS is the land surface model JSBACH (Raddatz et al., 2007; Brovkin et al., 2009; Reick et al., 2013; Schneck et al., 2013; Dalmonch and Zachle, 2013). It is typically used within the MPI-ESM (Giorgetta et al., 2013) and calculates the terrestrial storage of energy, water and carbon and its half-hourly exchanges between the atmosphere and the land surface. The variant of the model applied here is run uncoupled from the atmosphere and forced with reconstructed meteorology (see Sec. 3). The model considers ten plant functional types (PFTs: see Table 1). These PFTs are allowed to co-occur within one grid cell on different tiles, but nonetheless share a common water storage. Compared to the aforementioned JSBACH studies, the MPI-CCDAS does not use land-use change and land-use transition nor dynamic vegetation, but uses a multi-layer soil hydrology scheme (Hagemann and Stacke, 2014).

The application of gradient-based minimisation procedures is facilitated by a differentiable implementation of  $J(p)$ . To improve differentiability, the original phenology scheme, which describes the timing and amount of foliar area based on logistic growth functions (Lasslop, 2011) was replaced by the alternative scheme developed explicitly for this purpose (Knorr et al., 2010) (see Sec. 2.2.1). Some further minor modifications were necessary to make the code differentiable. These changes included replacing look-up tables with their continuous formulations, avoiding division by zero in the derivative code (e.g. through evaluation of  $\sqrt{0}$  in the forward mode), and reformulating minimum and maximum calculations to allow a smooth transition at the edge. These modifications alter the calculations, however, they were implemented such that the differences in the modelled results compared to the original code is minimal.

### 2.2.1 Phenology-module

In the revised MPI-CCDAS phenology scheme (Knorr et al., 2010), each plant functional type is assigned to a specific phenotype, implying limitations on phenology by water (tropical and raingreen PFTs), water and temperature (herbaceous PFTs) and temperature and daylight (extra-tropical tree PFTs; see Table 1). The evolution of the leaf area index  $\Lambda$  (LAI) on a daily time-step  $\Delta t$  is described as

$$\Lambda(t + \Delta t) = \Lambda_{lim} - [\Lambda_{lim} - \Lambda(t)]e^{-r\Delta t} \quad (2)$$

Table 1. Plant functional types that are optimised and the limitations that control the phenological behaviour of the respective functional type.

Plant functional type	Limitations
Tropical evergreen trees (TrBE)	Water
Tropical deciduous (TrBS)	
Raingreen shrubs (RS)	
Coniferous evergreen trees (CE)	Temperature and Daylight
Extra-tropical deciduous trees (ETD)	
Coniferous deciduous (CD)	Temperature and Water
C3-grasses (TrH)	
C3-crops (TrCr)	
C4-crops (TrCr)	

with the inverse time scale  $\tau$ , which is defined as:

$$r = \xi f + (1 - f)/\tau \quad (3)$$

The parameter  $\xi$  describes the rate of initial leaf growth, and the parameter  $\tau$  describes how quickly leaves are shed.  $f$  specifies the stage of the vegetation being fully active at  $f = 1$  or fully dormant at  $f = 0$  (see Eq. 5).  $\Lambda_{lim}$  is defined as:

$$\Lambda_{lim} = \xi \Lambda_{max} f / \tau \quad (4)$$

where the parameter  $\Lambda_{max}$  is the maximum allowed LAI.

The scheme accounts for grid-cell heterogeneity by smoothly varying the vegetation's state  $f$  between the two extremes. The transition is controlled either by the length of the day  $t_d$  or a smoothly averaged temperature  $T_m$  with a "memory"-time scale of 30 days (for details see Knorr et al. (2010)).

$$f = \Phi\left(\frac{T_m - T_\phi}{T_r}\right) \Phi\left(\frac{t_d - t_c}{t_r}\right) \quad (5)$$

with the temperature control parameters  $T_\phi$ ,  $T_r$  and day-length control parameters  $t_c$  and  $t_r$  and the cumulative normal distribution  $\Phi$ .

Water limitation is incorporated by calculating a water-limited maximum leaf area index  $\Lambda_W$  that cannot be exceeded by the actual LAI:

$$\Lambda_W = \frac{W \Lambda^{last}}{E_{pot} \tau_W} \quad (6)$$

with a water limitation time scale  $\tau_W$ . The potential evaporation  $E_{pot}$ , the relative root-zone moisture  $W$  and the LAI  $\Lambda^{last}$  are taken from the previous day averages.  $\Lambda_W$  is also applied with a memory time-scale of 30 days, similar to temperature and day length.

*what does this actually mean?*

$$i.e. \Lambda^{(t)} = \max(\Lambda(t), \Lambda_W)$$

*unclear*



4

Schürmann et al.: MPI-CCDAS

## 2.2.2 Photosynthesis

Photosynthesis in JSBACH follows Farquhar et al. (1980) for C3-plants and Collatz et al. (1992) for C4-plants, with details as described in Knorr and Heimann (2001) and Knorr (1997). Net leaf CO<sub>2</sub> uptake is the minimum of a carboxylation limited photosynthesis rate  $J_C$  and of electron transport limited rate  $J_E$  minus dark respiration  $R_d$ :

$$A = \min\{J_C, J_E\} - R_d \quad (7)$$

The carboxylation limited rate is calculated as:

$$J_C = V_m \frac{C_i - \Gamma_*}{C_i + K_C(1 + O_m/K_O)} \quad (8)$$

with the leaf internal CO<sub>2</sub>-Concentration  $C_i$ , the oxygen concentration  $O_m$  (0.21 mol/mol) and the CO<sub>2</sub> compensation point (without dark respiration)  $\Gamma_* = 1.7 \mu\text{mol}/\text{mol}^\circ\text{C} * T$  which depends on temperature  $T$  (in °C).  $K_C$  and  $K_O$  are the Michealis-Menten constants for CO<sub>2</sub> and O<sub>2</sub> and  $V_m$  is the maximum carboxylation rate. The latter three all depend on the canopy temperature  $T_c$  (in K) in the form (exemplified for  $V_m$ ):

$$V_m = V_{c_{max}} * \exp\left(\frac{E_V T_0}{T_1 R_g T_c}\right) \quad (9)$$

with activation energy  $E_V = 58520 \text{ Jmol}^{-1}$ , gas constant  $R_g = 8.314 \text{ JK}^{-1}\text{mol}^{-1}$ .  $T_1 = 298.16 \text{ }^\circ\text{C}$  is a reference temperature and  $T_0 = T_c - T_1$  the difference to this reference.  $V_{c_{max}}$  is the maximal carboxylation rate at 25 °C and is given in Table C1. Temperature dependence of  $K_C$  and  $K_O$  are calculated with a similar approach with reference values at 25 °C for  $K_{C0} = 460 * 10^{-6} \text{ mol/mol}$  and  $K_{O0} = 330 * 10^{-3} \text{ mol/mol}$  and activation energies of  $E_C = 59356 \text{ Jmol}^{-1}$  and  $E_O = 35948 \text{ Jmol}^{-1}$ , respectively.

The electron transport limited rate,  $J_E$ , is calculated as

$$J_E = J \frac{C_i - \Gamma_*}{4(C_i - 2\Gamma_*)} \quad (10)$$

with

$$J = \frac{\alpha I J_m}{\sqrt{J_m^2 + \alpha^2 I^2}} \quad (11)$$

and the photon capture efficiency  $\alpha = 0.28 \text{ mol(electrons)/mol(photons)}$ , the absorption rate of photosynthetically active radiation  $I$ , and the limiting rate constant  $J_m$  with a temperature dependence:

$$J_m = J_{max} * T/25^\circ\text{C} \quad (12)$$

$J_{max}$  is the maximum rate of electron transport at 25 °C (Table C1).

Photosynthesis for C4-plants follows Collatz et al. (1992) and is the minimum among the three limiting rates  $J_e = V_m$ ,

$J_c = kC_i$  and  $J_i = \alpha_i I$  with the quantum efficiency  $\alpha_i = 0.04$  and  $k$ :

$$k = J_{max} * 10^8 \exp\left(\frac{E_K T_0}{T_1 R_g T_c}\right) \quad (13)$$

with  $E_K = 50967 \text{ Jmol}^{-1}$ .

Dark respiration is modelled depending on  $V_{c_{max}}$  according to

$$R_d = fr_{C3|C4} * V_{c_{max}} * \exp\left(\frac{E_R T_0}{T_1 R_g T_c}\right) \quad (14)$$

with activation energy  $E_R = 45000 \text{ Jmol}^{-1}$ , and  $fr_{C3|C4} = 0.011|0.031$  for C3 and C4 plants, respectively. Dark respiration is reduced to 50% of its value during light conditions (Brooks and Farquhar, 1985).

Photosynthesis and dark respiration are inhibited above 55°C. Calculations are performed per PFT and three distinct canopy layers, which vary in depth according to the current leaf area index, assuming that within the canopy nitrogen, and thus  $V_{c_{max}}$ ,  $J_{max}$ , and  $R_d$  decline proportionally with light levels in the canopy. PFT values are integrated to grid-cell averages according to the cover fractions of each PFT within each grid-cell.

## 2.2.3 Carbon-water coupling

JSBACH employs a two-step approach to couple the plant carbon and water fluxes (Knauer et al., 2015). Given a photosynthetic-pathway dependent specific maximal internal leaf CO<sub>2</sub> concentration ( $C_i$ ), a maximal estimate of stomatal conductance ( $g_{s_{pot}}$ ) is derived for each canopy layer, which is then reduced by a water-stress factor ( $w_s$ ) to arrive at the actual stomatal conductance ( $g_{s_{act}}$ ) (see Knorr, 1997, 2000, and references therein).

$$g_{s_{act}} = w_s * g_{s_{pot}} = w_s * 1.6 * \frac{A}{C_a - C_i} \quad (15)$$

where  $C_a$  and  $C_i$  are the external and internal leaf CO<sub>2</sub> concentrations. The water-stress factor  $w_s$  is defined as

$$w_s = \min\left(\frac{W_{root} - W_{witl}}{W_{crit} - W_{witl}}, 1\right) \quad (16)$$

where  $W_{root}$  is the actual soil-moisture in the root zone, and  $W_{crit|witl}$  define the soil moisture levels at which stomata begin to close, or reach full closure, respectively. Soil moisture and bare soil evaporation are calculated according to the multi-layer soil water scheme of Hagemann and Stacke (2014).

Given the water-stressed stomatal conductance, leaf internal CO<sub>2</sub> concentration and carbon assimilation are then recalculated for each canopy layer by solving simultaneously the diffusion equation and the photosynthesis equations as outlined above (Sec. 2.2.2)



Schürmann et al.: MPI-CCDAS

5

## 2.2.4 Land carbon pools, respiration and turnover

The vegetation's net primary production (NPP) is related to the net assimilation (A) as

$$NPP = A - R_m - R_g \quad (17)$$

where  $R_g$  is the growth respiration, which is assumed to be a fixed fraction (20%) of  $A - R_m$ .  $R_m$  is the maintenance respiration, which is assumed to be coordinated with foliar photosynthetic activity, and thus scaled to leaf dark respiration via  $f_{aut\_leaf}$  (Knorr, 2000)

$$R_m = \frac{R_d}{f_{aut\_leaf}} \quad (18)$$

with the dark respiration  $R_d$  as given in Eq. 14. As a consequence, an increase in  $f_{aut\_leaf}$  leads to an increase in NPP.

NPP is allocated to either a green or woody pool given fixed, PFT-specific allocation constants. The green pool turns over to litter according to the leaf phenology, whereas the woody turnover is prescribed as a fixed constant.

JSBACH considers three litter pools (above ground green, below ground green and woody) with distinct, PFT-specific turnover times, as well as a soil organic matter pool with a longer turnover time. Heterotrophic respiration for each of these pools responds to temperature according to a  $Q_{10}$  formulation:

$$R_{pool} = \alpha_{resp} * Q_{10}^{(T-T_{ref})/10} / \tau_{pool} * C_{pool} \quad (19)$$

with a soil-moisture dependent factor  $0 \leq \alpha_{resp} \leq 1$ .  $C_{pool}$  is either the slow soil carbon pool, above or below ground green litter or wood litter pool and  $T$  is temperature and  $T_{ref} = 0^\circ\text{C}$  the reference temperature and a pool depended turnover rate  $\tau_{pool}$  (more details on the carbon balance sub-module can be found in Goll et al., 2012).

## 2.2.5 Atmospheric transport

To map the net land-atmosphere  $\text{CO}_2$  exchange simulated by JSBACH to observations of the atmospheric  $\text{CO}_2$ -mole fraction, the computation of atmospheric transport is required. The transport model TM3 (Heimann and Körtner, 2003) is used for that. Specifically we compute the response of monthly mean  $\text{CO}_2$  mole fractions to monthly mean surface fluxes (extending 2 years back in time) and multiply these transport matrices (or Jacobians) with the net  $\text{CO}_2$  exchange as in Rödénbeck et al. (2003). The net exchange is the sum of the terrestrial fluxes computed by JSBACH and prescribed ocean and fossil fuel fluxes. The mole fraction at the beginning of this simulation is specified as a globally constant offset  $\text{CO}_2^{offset}$ , one of the parameters to be estimated. The resulting  $\text{CO}_2$ -mole fractions can then be directly compared with observed atmospheric  $\text{CO}_2$ .

## 2.3 Model parameters

In the presented set-up, JSBACH parameters related to the phenology, photosynthesis and land carbon turnover (including initial carbon stocks) are estimated. The default prior value and assumed prior uncertainty (with Gaussian distribution) of each parameter, as well as posterior values from the assimilation experiments are given in Table 2. The choice of these parameters was based on an extensive parameter sensitivity study on a much larger set of parameters across multiple biomes (Schürmann, unpublished results). We retained those parameters, for which we found a significant effect on modelled FAPAR and net  $\text{CO}_2$  exchange. In principle, it is possible to add more parameters, which are decisive for other modelled quantities such as soil moisture and which might feed back to our observables.

The parameters controlling the phenology ( $\Lambda_{max}$ ,  $1/\eta$ ,  $\tau_w$ ,  $T_\phi$  and  $t_d$ ) are allowed to take different values for different plant functional types with the exception of  $\xi$ , which is valid globally. Their parameter prior values and uncertainties are taken from Knorr et al. (2010), with the following three exceptions: the water control parameter  $\tau_w$  required an adaptation to account for the different soil-water formulations in the MPI-ESM compared to BETHY,  $1/\eta$  for the coniferous evergreen (CE) PFT also has been adapted after preliminary site-scale studies to allow more flexibility in the seasonality of the evergreen-phenology (Schürmann, unpublished results) and, finally,  $\Lambda_{max}$  is left to its default JSBACH parameter value for all PFT's with the exception of the coniferous evergreen (CE) PFT. For this PFT a value of  $\Lambda_{max} = 1.7 \text{ m}^2/\text{m}^2$  has been used, because preliminary model tests revealed a large bias in modelled FAPAR in CE-dominated regions (see also Sect. 5.3.2).

To estimate gross assimilation directly, maximum carboxylation rate  $V_{cmax}$  and maximum electron transport  $J_{max}$  are allowed to change per plant functional type. We reduce the number of parameters to be estimated, assuming that the observed tight correlation between  $V_{cmax}$  and  $J_{max}$  is conserved irrespective of the precise value for each PFT (Katge and Knorr, 2007). Thus, we introduce a single scaling coefficient  $f_{photos}$ :

$$V_{cmax} = V_{cmax}^{prior} * f_{photos} \quad (20)$$

$$J_{max} = J_{max}^{prior} * f_{photos} \quad (21)$$

Prior parameter ranges for each PFT were derived from the TRY data-base Katge et al. (2011).

The prior sensitivity studies revealed that the most influential parameters controlling C storage on land and partitioning between autotrophic and heterotrophic respiration were the leaf fraction of maintenance respiration ( $f_{aut\_leaf}$ ) and temperature response ( $Q_{10}$ ) of the carbon pools, which were both included as parameters. In addition, we accounted for non steady-state conditions of the net carbon flux by estimat-

or optimized!

rate



Table 2. Parameters that are part of the control vector with their prior and posterior values of the global assimilation experiments. Parameters marked with a \* are multiplied with their respective value in the model, given in Table C1. The mapping variants are explained in the appendix B: 1: No lower bound; 2: A lower bound at 0 for those parameters that are not allowed to take negative values.

Parameter(PFT)	Description	Prior sigma	Prior	JOINT	CO2alone	FAPARalone	Unit	Mapping
$\Lambda_{max}$ (TrBE)*	Maximum LAI	0.2	1	0.98	0.82	0.84	.	2
$\Lambda_{max}$ (TrBD)*	Maximum LAI	0.2	1	0.58	0.55	0.63	.	2
$\Lambda_{max}$ (ETD)*	Maximum LAI	0.2	1	0.98	1.04	1.44	.	2
$\Lambda_{max}$ (CE)*	Maximum LAI	0.2	1	1.00	0.84	1.01	.	2
$\Lambda_{max}$ (CD)*	Maximum LAI	0.2	1	0.64	1.31	0.56	.	2
$\Lambda_{max}$ (RS)*	Maximum LAI	0.2	1	1.33	0.94	1.24	.	2
$\Lambda_{max}$ (TeH,TeCr)*	Maximum LAI	0.1	1	0.63	0.53	0.61	.	2
$\Lambda_{max}$ (TrH,TrCr)*	Maximum LAI	0.1	1	0.53	0.49	0.59	.	2
$1/\tau$ (ETD)	Leaf shedding time scale	0.01	0.07	0.057	0.057	0.079	d <sup>-1</sup>	2
$1/\tau$ (CE)	Leaf shedding time scale	1e-04	5e-04	0.00067	0.00045	0.00064	d <sup>-1</sup>	2
$1/\tau$ (CD)	Leaf shedding time scale	0.01	0.07	0.068	0.07	0.068	d <sup>-1</sup>	2
$1/\tau$ (TeH,TeCr)	Leaf shedding time scale	0.01	0.07	0.098	0.076	0.079	d <sup>-1</sup>	2
$1/\tau$ (TrH,TrCr)	Leaf shedding time scale	0.01	0.07	0.077	0.07	0.07	d <sup>-1</sup>	2
$\tau_w$ (TrBE)	Water stress tolerance time	30	300	319.82	378.04	286.77	days	2
$\tau_w$ (TrBD)	Water stress tolerance time	10	114	107.78	120.84	106.29	days	2
$\tau_w$ (RS)	Water stress tolerance time	5	50	49.51	50.02	47.82	days	2
$\tau_w$ (TeH,TeCr)	Water stress tolerance time	25	250	222.32	215.22	230.41	days	2
$\tau_w$ (TrH,TrCr)	Water stress tolerance time	25	250	276.06	236.32	286.64	days	2
$T_\phi$ (ETD)	Temperature at leaf onset	1	9.21	7.19	8.63	2.28	°C	1
$T_\phi$ (CE)	Temperature at leaf onset	1	9.21	7.53	9.01	7.61	°C	1
$T_\phi$ (CD)	Temperature at leaf onset	1	9.21	0.10	5.53	0.30	°C	1
$T_\phi$ (TeH,TeCr)	Temperature at leaf onset	0.5	1.92	3.82	2.67	2.78	°C	1
$T_\phi$ (TrH,TrCr)	Temperature at leaf onset	0.5	1.92	2.50	1.57	1.88	°C	1
$t_a$ (ETD)	Day length at leaf shedding	1	13.37	13.57	13.84	13.60	hours	2
$t_a$ (CE)	Day length at leaf shedding	1	13.37	14.22	13.69	14.12	hours	2
$t_a$ (CD)	Day length at leaf shedding	1	13.37	14.94	13.66	14.73	hours	2
$\xi$	Initial leaf growth rate	0.03	0.37	0.41	0.38	0.43	d <sup>-1</sup>	2
$f_{photos}$ (TrBE)*	Photosynthesis rate modifier	0.1	1	0.75	1.02	0.91	.	2
$f_{photos}$ (TrBD)*	Photosynthesis rate modifier	0.1	1	1.07	1.08	0.97	.	2
$f_{photos}$ (ETD)*	Photosynthesis rate modifier	0.02	1	0.99	1.00	1.00	.	2
$f_{photos}$ (CE)*	Photosynthesis rate modifier	0.03	1	0.95	1.00	1.00	.	2
$f_{photos}$ (CD)*	Photosynthesis rate modifier	0.06	1	1.04	1.05	1.00	.	2
$f_{photos}$ (RS)*	Photosynthesis rate modifier	0.1	1	1.01	1.05	1.00	.	2
$f_{photos}$ (TeH)*	Photosynthesis rate modifier	0.1	1	0.96	1.01	0.99	.	2
$f_{photos}$ (TeCr)*	Photosynthesis rate modifier	0.1	1	0.67	0.86	1.00	.	2
$f_{photos}$ (TrH)*	Photosynthesis rate modifier	0.1	1	1.04	1.02	1.06	.	2
$f_{photos}$ (TrCr)*	Photosynthesis rate modifier	0.1	1	0.87	0.94	1.00	.	2
$Q_{10}$	Temperature sensitivity of resp.	0.15	1.8	1.90	1.81	1.80	.	2
$f_{atow}$	Multiplier for initial slow pool	0.1	1	0.50	0.51	1.00	.	2
$f_{aut\_leaf}$	Leaf fract. of maintenance resp.	0.1	0.4	0.30	0.35	0.40	.	2
$CO_2^{isset}$	Initial atmospheric carbon	3	0	0.90	0.85	0.00	ppm	1

Is this Cpr?

is this Ppr?

Ppo



Schürmann et al.: MPI-CCDAS

ing a global scaling factor for the size of the initial slow pool  $f_{slow}$ , the same approach as used by Carvalhais et al. (2008). This allows for the modification of global heterotrophic respiration and hence also an adjustment of the  $CO_2$  growth rate, but the limitation is that this does not change the spatial distribution of carbon pools, which remains controlled by the prior parameter values. The turnover-time parameters (see Eq. 19) were not included in the assimilation experiment, because their impact on land carbon fluxes was small compared to other parameters (Schürmann, unpublished results) at the time-scale of the MPI-CCDAS (a couple of years). To give flexibility to the assimilation system for the initial carbon content of the atmosphere, one single offset value  $CO_2^{offset}$  is included in the set of estimated parameters. The uncertainties of these last parameters ( $Q_{10}$ ,  $f_{out\_leaf}$ ,  $f_{slow}$  and  $CO_2^{offset}$ ) are based on expert knowledge.

Further, uncertainties on all parameters were assumed to be Gaussian and exposed to the assimilation procedure in a form normalized by their prior uncertainty. In order to prevent parameters from attaining physically impossible, negative values, some parameters were constrained at the lower end of the distribution to zero (see Table 2 and appendix B).

## 2.4 Observational constraints and observation operators

### 2.4.1 Atmospheric $CO_2$

Observed atmospheric  $CO_2$  mole fractions were obtained from the flask data/continuous measurements provided by different institutions (e.g. flask data of NOAA/CMDL's sampling network, update of Conway et al. 1994, Japan Meteorological Agency - JMA, Meteorological Service of Canada - MSC, and many others; see Rödenbeck et al. 2003). Stations were selected in order to cover representatively a latitudinal gradient (Table A1), focussing on remote locations with little imprint of local fluxes. For cross-evaluation, a wider set of available station data were used (Table A2). The temporal resolution of the  $CO_2$  original data at the monitoring stations (hourly to daily/weekly) depends on the specific station and were averaged into monthly means.

For our analysis, we used the Jacobian representation of the TM3 model, version 3.7.24 (Rödenbeck et al., 2003), with a spatial resolution of about  $4^\circ \times 5^\circ$  (the "fine" grid of TM3 by Heimann and Körner 2003), driven by interannually varying wind fields of the NCEP reanalysis (Kalnay et al., 1996). The MPI-CCDAS compares atmospheric  $CO_2$  at a monthly temporal resolution, considering the sampling of simulated  $CO_2$  abundance at the same time in which measurements were available in order to reduce the representation bias. The treatment of the observations of  $CO_2$  and their uncertainties are done as in Rödenbeck et al. (2003). A floor value of 1 ppm is added to this uncertainty, similarly as in Rayner et al. (2005). Ancillary flux fields at monthly resolution were used to represent the ocean (Jena CarboScope

pCO<sub>2</sub>-based mixed layer scheme oc\_v1.0 Rödenbeck et al., 2013) and fossil fuel (Emissions Database for Global Atmospheric Research EDGAR; <http://edgar.jrc.ec.europa.eu>) net  $CO_2$  fluxes.

### 2.4.2 TIP-FAPAR

The observations of FAPAR that have been assimilated were specifically derived for this study by the Joint Research Centre Two-stream Inversion Package (JRC-TIP, Pinty et al. 2007). The product was derived by running JRC-TIP on MODIS broadband visible and near-infrared white sky surface albedo input aggregated to the model grid separately for snow-free and snow-like background conditions in a similar way as described for the native 0.01 degree product (Pinty et al., 2011a, b; Clerici et al., 2010; Voßbeck et al., 2010). Uncertainties in the FAPAR data are based on rigorous uncertainty propagation using first and second derivative information (Voßbeck et al., 2010).

We apply two filters on the global FAPAR product to assure that potential model structural errors do not lead to compensating effects in the parameter estimation procedure and thus impede fitting the FAPAR data in other regions. First, owing to the fact that no specific crop-phenology is implemented in JSBACH, grid cells with fractional crop coverage of more than 20 % have been filtered out, as we cannot expect the model to fit cropland phenology. Second, grid-points with correlations between the prior model and the observed FAPAR below 0.2 (i.e. prior phenology exhibits out-of-phase seasonal cycles) have also been filtered out. Together, these filters reduce the overall global coverage of the FAPAR-constraint and thus the number of observations to be fitted (Fig. 1) by 57 %.

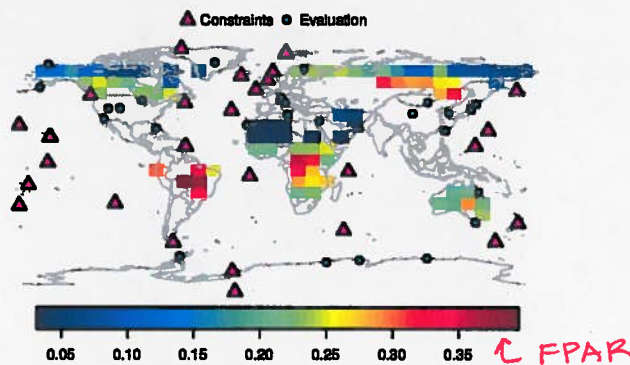


Figure 1. Location of the  $CO_2$  observations (for constraining the model and for evaluation) and the median over the time series of the TIP-FAPAR uncertainties in each pixel acting as constraint

Is this what the colour-bar represents. FAPAR varies between 0 and 1 so these uncertainties seem large.

how?

Table A2 doesn't look any longer than A1.

Aren't the atmos-ocean  $CO_2$  fluxes prescribed? This seems to suggest you are doing something more.



8

Schürmann et al.: MPI-CCDAS

### 3 Experimental set-up

The MPI-CCDAS is driven by daily meteorological forcing (air temperature, specific humidity, precipitation, downward short- and longwave radiation, wind speed) obtained from the WATCH forcing data set (Weedon et al., 2014). Annual CO<sub>2</sub> mole fractions of the atmosphere as a forcing for the photosynthesis calculations of JSBACH were prescribed according to Sitch et al. (2015). Vegetation distribution (Fig. D1) and other surface characteristics are derived from Pongratz et al. (2008). For computational efficiency, we have set-up the MPI-CCDAS at a coarse spatial resolution (the "coarse" grid of TM3 by Heimann and Köhler 2003 with about 8°x10°), although the MPI-CCDAS is flexible to be run at any computationally feasible spatial resolution.

For the water and carbon cycle state-variables of JSBACH the following spin up procedure was applied: First, an equilibrium was achieved through an integration over the period 1979-1989 with corresponding meteorological forcing and atmospheric CO<sub>2</sub> mole fractions of 1979. From this equilibrium state a transient integration from 1979 to 2003 followed. The final state of 2003 was then taken as the initial condition for all MPI-CCDAS experiments. This spin-up procedure used the prior parameter values, i.e. it was not part of the assimilation loop for the parameter estimation. To allow a direct control of the non-equilibrium states of the carbon pools, the initial slow pool (at the end of the spin-up procedure) was multiplied by a global scaling factor that is part of the parameter estimation procedure (see Sect. 2.3).

The MPI-CCDAS itself was run for the years 2003 - 2011, i.e. parameters were left free to adapt to the observational constraints. The first two years allowed the system to build a spatial gradient in the simulated CO<sub>2</sub> mole fractions. In the following years (2005 and 2009) the observational constraints were active whereas for the consecutive two years (2010/2011) the constraints were inactive and the observations of these years serve for evaluation purposes (hindcasting). As evaluation statistics we used the correlation, bias, root mean squared error and the Nash-Sutcliffe model efficiency (NSE) which is defined as:

$$NSE = 1 - \frac{\sum_i (d_i - m_i)^2}{\sum_i (d_i - \bar{d}_i)^2} \quad (22)$$

with model  $m$ , observation  $d$ , the index  $i$  for individual pairs of observation and model output and an overbar denoting the arithmetic mean.  $NSE = 1$  indicates a perfect model and for all  $NSE < 0$  the mean of the observations is a better predictor than the model itself.

Our study follows a factorial design to assess the benefit of each data stream, but also to evaluate the potential of assimilating more than one data stream and its effect on the carbon cycle. Therefore, we conducted three experiments: an experiment assimilating each data stream alone (CO<sub>2</sub>alone using only CO<sub>2</sub> and FAPARalone using only TIP-FAPAR

and one experiment assimilating both data streams simultaneously (JOINT), with each data stream equally weighted.

### 4 Results

#### 4.1 Performance of the assimilation

The application of the MPI-CCDAS to the given problem was successful within an appropriate number of iterations (with run-times of 1 - 2 months), increasing from FAPARalone (using only TIP-FAPAR), to CO<sub>2</sub>alone (using only CO<sub>2</sub>), and JOINT (using both observations simultaneously as a constraint; Table 3): For all three assimilation experiments, the value of the cost-function was considerably reduced, while the posterior parameter values remained in physically plausible ranges, even though a few (e.g.:  $T_{\phi}$  of the coniferous deciduous phenotype) deviate strongly from the prior values (Table 2). For FAPARalone, the cost was almost halved between prior and posterior run. Yet stronger reductions of the cost were obtained in the other two experiments using also CO<sub>2</sub> (Table 3). Interestingly, the posterior cost of the JOINT assimilation roughly equals the sum of the single data-stream experiments, indicating consistency of the model with both data streams. Several statistics comparing the posterior model with observations for FAPAR and CO<sub>2</sub> (Tables 4 and 5) show that the model performance of the JOINT experiment was comparable to the performance of the two single data-stream experiments relative to the assimilated quantity. While the JOINT assimilation captured the main features of both data sources, the single data-stream assimilation experiments either showed no improvement with respect to the other data stream (such as the CO<sub>2</sub>alone case for FAPAR), or even a degradation (such as the FAPARalone case for CO<sub>2</sub>). Overall, these results suggest that both data streams can be successfully assimilated jointly with the MPI-CCDAS.

During the assimilation procedure, the norm of the gradient<sup>1</sup> was considerably reduced by 3 - 4 orders of magnitude (Table 3). The behaviour was such that in the first tens of iterations, the assimilation considerably reduced the cost as well as the norm of the gradient. The parameter values changed the most in this initial phase of the assimilation. However, they also changed in later iterations without substantial reductions in the cost function or the norm of the gradient. The assimilation then finally stopped because the changes to the parameters were too small. Notably, the norm did not approach zero for the cases using CO<sub>2</sub> as a constraint, as would have been expected for the minimum of the cost-function. This is an indication that for these experiments our posterior parameter estimate does not yet minimize the cost function: a point also mentioned by Rayner et al. (2005) with respect to their CO<sub>2</sub> assimilation with the BETHY-CCDAS. In the fol-

<sup>1</sup>The norm of a vector  $v$  is:  $\|v\| = \sqrt{v \cdot v}$

*spatial resolution*

*what is initial slow pool*

*unclear*

*function*

*gradient of what*

*iterations of what*

*Does this mean that if the model were to run longer after 2011 then it will drift and go back to its prior state?*



**Table 3.** Characteristics of the assimilation experiments. The prior and posterior cost-function values and the contribution of FAPAR, CO<sub>2</sub> and the prior (second term in Eq. 1) to the posterior cost-function value are given as well as the norm of the gradient and the number of observations acting as a constraint and the number of iterations of the assimilation

Experiment name	Prior cost	Posterior cost	FAPAR cost	CO <sub>2</sub> cost	Parameter cost	Prior norm of the gradient	Posterior norm of the gradient	Number of observations	Number of iterations
CO2alone	1922	344	0	287	57	12196	14.8	1524	69
FAPARalone	1431	723	626	0	97	208	0.7	3189	29
JOINT	3352	1102	682	309	112	12162	6.1	4713	69

lowing we discuss the performance of the assimilation with respect to FAPAR and CO<sub>2</sub> in detail.

#### 4.2 Phenology

The statistics of the comparison with the TIP-FAPAR data sets shows an improvement of the model-data fit for all experiments relative to the prior model (Table 4), which as expected is strongest when using FAPAR (FAPARalone and JOINT) as a constraint.

One important aspect in the improvement was a general, time-averaged, reduction in modelled FAPAR simulated by the MPI-CCDAS compared to the prior run. This change in FAPAR was mostly driven by a reduction of foliar area of  $0.41 \text{ m}^2\text{m}^{-2}$  on average for the JOINT experiment ( $0.34 \text{ m}^2\text{m}^{-2}$  for FAPARalone and  $0.59 \text{ m}^2\text{m}^{-2}$  for CO2alone). Almost all PFTs contributed to the decrease in FAPAR following a reduction in the maximum leaf area index (parameter  $\Lambda_{max}$ ) for tropical deciduous forests, needle-leaf deciduous forests, as well as herbaceous PFTs (crops and grasses). The water-stress parameter  $\tau_w$  played a secondary role in the reduction, affecting the maximum leaf-area for drought responsive phenologies (see Table 1). The concurrent increase of foliar area for extra-tropical deciduous and rain green shrubs only plays a minor role in the model-data agreement, since these PFTs only cover a small fraction of the global land area.

In regions with a strong temperature control of phenology, the assimilation did not only change the magnitude of the phenological seasonal cycle, but also its timing, reflected in the improved correlation and model efficiency of the MPI-CCDAS with respect to the TIP-FAPAR data (Table 4). This improvement was mostly the result of adjusting the parameters  $T_\phi$  and  $t_c$ , which denote temperature and day-length criteria that determine when the vegetation alters from the dormant to the active phase. The reduction of the temperature control parameter  $T_\phi$  leads to an earlier onset of the growing season in the extra-tropical deciduous broadleaf and deciduous needleleaf PFTs. For the deciduous evergreen forests the assimilation procedure also resulted in an earlier end of the growing season (see Fig. 2 for an example). For the other PFTs, these parameters changed not as pronounced, leading to no notable difference in the phenological timing - at least not at the analysed monthly temporal resolution. No-

tably, also the CO2alone experiment shows some improvement in the correlation and model efficiency compared to TIP-FAPAR, although this experiment did not use the TIP-FAPAR data as a constraint. This suggests that the seasonal cycle of CO<sub>2</sub> bears some constraint on the timing of Northern extra-tropical phenology.

While the FAPARalone assimilation run performs best compared with TIP-FAPAR (Table 4), the FAPARalone and JOINT assimilation runs are fairly similar (though not identical) with respect to the simulated FAPAR. The temporally averaged LAI (Fig. 3) demonstrates the overall similarity between the FAPARalone and JOINT experiments. This similarity is also reflected in the parameter values of the phenology: the parameters of FAPARalone and JOINT often were closer to each other than to CO2alone (Table 2). However, the values are not necessarily the same, because different parameter combinations can lead to fairly similar results (also known as equifinality). This can happen when (i) certain parameters enter an insensitive regime where parameter differences do hardly propagate to the modelled foliar area, (ii) mixed pixels are a composite of different plant functional types that can show compensating effects, and (iii) the CO<sub>2</sub> constraint may still impose an additional weight on changing FAPAR because of the feedbacks on photosynthesis. An example for this is the tropical evergreen tree PFT, for which parameters of the JOINT and FAPARalone experiment are different while the modelled foliar area is very similar. A further explanation for this feature highlighting the importance of multi-data stream assimilation is given in Sec. 4.4.1. The most pronounced differences between the JOINT and FAPARalone experiment, leading also to the differences in the globally averaged foliar area, arose at locations where TIP-FAPAR data were not used as constraints in e.g. crop dominated pixels (where also the extra-tropical deciduous tree (ETD) PFT covered a substantial part of the grid-cell).

Larger differences were reached between the CO2alone and JOINT experiments (Table 4 and Fig. 3). CO2alone shows the smallest LAI, and thus the smallest FAPAR. This feature is especially pronounced in tropical regions, where the decrease is driven by the water-control parameter  $\tau_w$  and the maximum foliar area  $\Lambda_{max}$ . This pattern is countered by larger foliar area than the JOINT experiment for coniferous deciduous trees, driven by the parameter  $\Lambda_{max}$  which is increased for CO2alone, but decreased for the other two ex-

*is this globally averaged?*

*how is FAPAR simulated if it is being assimilated.*

*What is this? How can a forest be deciduous and evergreen at the same time?*

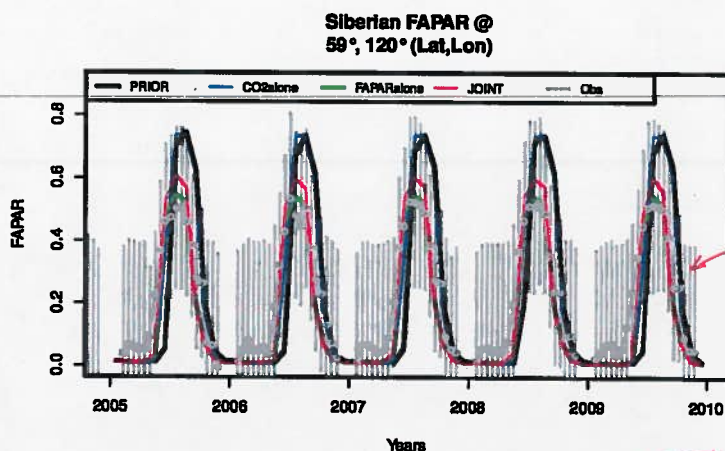


Figure 2. Example time-series of FAPAR for an East Siberian pixel dominated by the CD-PFT to demonstrate the improvement in the timing of the phenology after the assimilation. TIP-FAPAR observations are given with their  $1-\sigma$  uncertainties

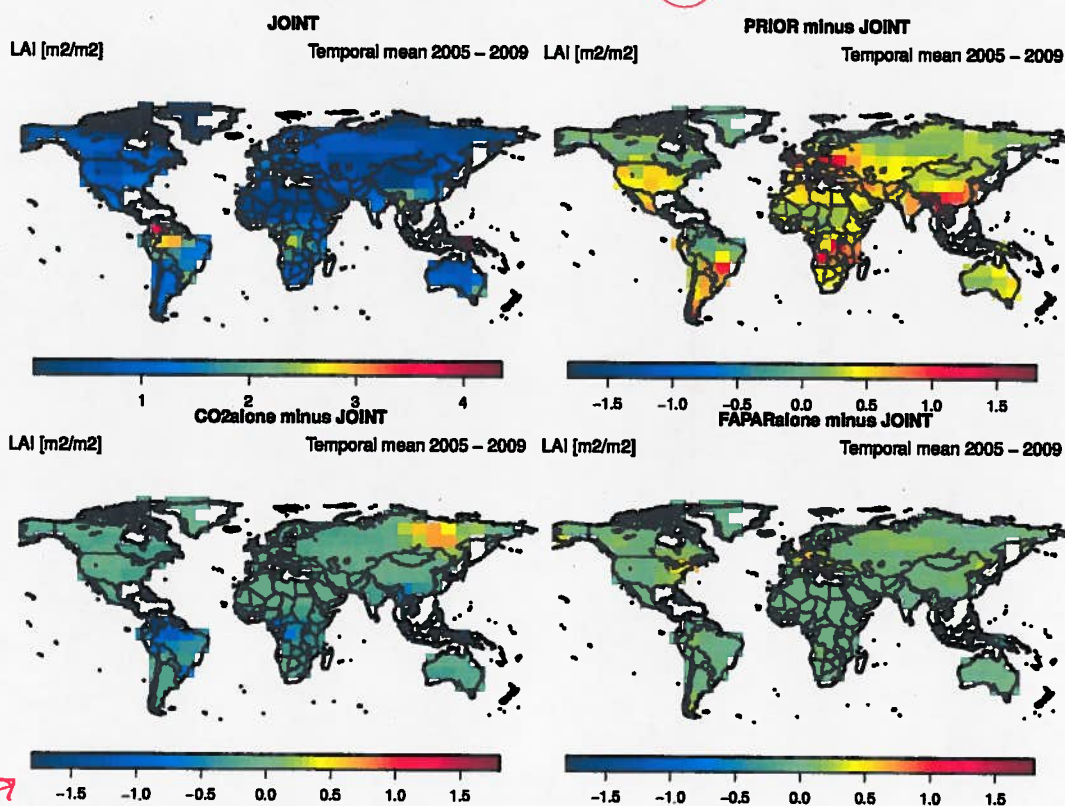


Figure 3. Temporally averaged global LAI of the JOINT experiment and differences of the other experiments to the JOINT case.

*very bad choice of colours.*



**Table 4.** Performance of the prior and posterior models compared with TIP-FAPAR observations (applying the same data quality screening as for the assimilation). The assimilation period (2005 - 2009) as well as a subsequent evaluation period (2010/2011) is shown. Abbreviations are: Corr: Correlation, RMSE: Root mean squared error, NSE: Nash Sutcliffe model efficiency.

	2005 - 2009				2010/2011			
	Corr	Bias	RMSE	NSE	Corr	Bias	RMSE	NSE
PRIOR	0.60	0.069	0.19	0.10	0.61	0.075	0.19	0.12
CO2alone	0.66	-0.072	0.17	0.31	0.67	-0.074	0.17	0.31
FAPARalone	0.72	-0.014	0.14	0.51	0.73	-0.013	0.14	0.52
JOINT	0.71	-0.022	0.14	0.49	0.72	-0.022	0.14	0.50

periments. A likely explanation of this behaviour is given in Sect. 4.4.2.

### 4.3 Atmospheric CO<sub>2</sub>

The assimilation procedure strongly reduced the misfit between observed and modelled atmospheric mole fraction of CO<sub>2</sub> when using CO<sub>2</sub> as a constraint (Table 5). This was true for the seasonal cycle, the seasonal cycle's amplitude and the 5-years trend (Fig. 4 and 5). Conversely, the FAPARalone experiment showed a strong deterioration of the simulated atmospheric CO<sub>2</sub> compared to the prior model, leading to a much faster increase in CO<sub>2</sub> than observed (Table 5 and Fig. 4). The deterioration of the 5-years trend of atmospheric CO<sub>2</sub> in the FAPARalone case occurred notwithstanding the improvement of the seasonal cycle amplitude of atmospheric CO<sub>2</sub> (Fig. 5). Notably, introducing TIP-FAPAR as an additional constraint in the JOINT experiment did not deteriorate the fit to the observed CO<sub>2</sub>. Rather, the simulated monthly CO<sub>2</sub> mole fractions of the JOINT and CO2alone experiment are almost identical for most sites (Table 5 and Fig. 4 and 5).

The improvement of the simulated atmospheric CO<sub>2</sub> for the CO2alone and JOINT assimilation run persisted for the two years following the assimilation period, in which the model was run in a hindcast mode (driven by reconstructed meteorology), with only minor degradation in model performance (Table 5). Both experiments clearly outperform the prior model, which is most obvious in the improvement of the Nash-Sutcliffe model efficiency for the hindcast period.

The comparison of the simulated posterior atmospheric CO<sub>2</sub> mole fractions at the evaluation stations showed a general improvement in the performance measures, with substantial improvements in the simulated bias, RMSE and Nash-Sutcliffe model efficiency relative to the prior model (Table 5). Unlike for the set of calibration sites, there was no difference in the improvement between the assimilation period and the subsequent two-year period, suggesting that the model improvement is of general nature. In other words, the prognostic capabilities of the model have been largely improved after assimilating CO<sub>2</sub>-observations, also at the evaluation locations.

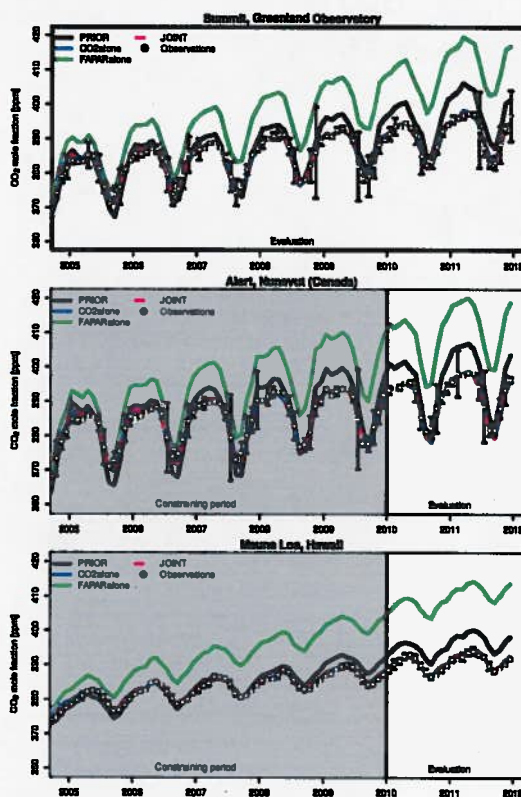


**Figure 4.** Time series of CO<sub>2</sub> as observed at the high latitude evaluation site Summit and at two constraining sites, one at high latitudes (Alert) and one representative for the Northern Hemisphere (Mauna Loa) for the different prior and posterior models. The observations are given together with their uncertainty.

#### 4.3.1 Changes in C fluxes causing the changes in simulated CO<sub>2</sub>

The changes in simulated atmospheric CO<sub>2</sub> mole fractions originate from substantial changes of the seasonal ampli-



**Table 5.** Performance of the prior and posterior models compared with atmospheric CO<sub>2</sub> for constraining and evaluation sites and for the assimilation period (2005 - 2009) and the hindcast period (2010/2011). Abbreviations are: Corr: Correlation, RMSE: Root mean squared error, NSE: Nash Sutcliffe model efficiency.

	2005 - 2009				2010/2011			
	Corr	Bias	RMSE	NSE	Corr	Bias	RMSE	NSE
<b>Stations acting as constraint</b>								
PRIOR	0.95	0.64	2.60	0.68	0.93	4.85	5.22	-0.69
CO2alone	0.96	-0.05	1.32	0.92	0.93	0.10	1.47	0.87
FAPARalone	0.91	8.91	9.84	-3.63	0.91	18.21	18.35	-19.86
JOINT	0.96	-0.09	1.35	0.91	0.93	-0.16	1.48	0.87
<b>Stations withheld from assimilation</b>								
PRIOR	0.86	1.20	3.83	0.52	0.84	5.18	6.03	-0.61
CO2alone	0.89	0.25	2.54	0.79	0.89	0.19	2.19	0.79
FAPARalone	0.84	9.73	10.84	-2.87	0.86	18.89	19.12	-15.14
JOINT	0.88	0.24	2.61	0.78	0.88	-0.05	2.28	0.77

**Table 6.** Global averages of selected carbon cycle components in PgCyr<sup>-1</sup> for fluxes and PgC for stocks and comparison with other estimates. Ra: autotrophic respiration. Rh: heterotrophic respiration. Reco: ecosystem respiration.

	PRIOR	CO2alone	FAPARalone	JOINT	Other estimates	Other CCDAS
NPP	65.5	40.9	53.5	45.6	44 - 66 <sup>a</sup>	40 <sup>a</sup>
Ra	86.1	57.6	67.8	65.7		
Rh	64.5	37.6	55.4	42.2		
Reco	150.6	95.2	123.2	107.9		
GPP	151.6	98.4	121.3	111.3	119 ± 8 <sup>b</sup> , 123 ± 8 <sup>c</sup>	109 - 164 <sup>h</sup>
NBP	1	3.2	-2.2	3.2	2.4 ± 0.8 <sup>d</sup>	
Soil Carbon	2649	1064.7	2187.1	1122.3	1343 <sup>e</sup>	
Vegetation Carbon	424	388.5	420.5	407.3	442 ± 146 <sup>f</sup>	
Litter Carbon	239.9	189.8	212.8	193.9		

<sup>a</sup>Cramer et al. (1999); Saugier and Roy (2001); <sup>b</sup>Jung et al. (2011); <sup>c</sup>Beer et al. (2010); <sup>d</sup>Le Quéré et al. (2015);

<sup>e</sup><http://web.archive.iiasa.ac.at/Research/LUC/External-World-soil-database/HTML/>; <sup>f</sup>Carvalho et al. (2014); <sup>g</sup>Rayner et al. (2005); <sup>h</sup>Koffi et al. (2012)

tude and the strength of the net carbon fluxes of JSBACH. The application of the CO<sub>2</sub>-constraint increased the global net biome production (NBP) from 1.0 PgCyr<sup>-1</sup> in the prior model to 3.2 PgCyr<sup>-1</sup> in the CO2alone and JOINT experiments, whereas it decreased the net uptake to -2.2 PgCyr<sup>-1</sup> for the FAPARalone case, turning the biosphere into a net source (Table 6). While the atmospheric observations constrain the net land-atmosphere CO<sub>2</sub> flux, the MPI-CCDAS model parameters affect the gross-fluxes, and thus the changes in NBP are again the consequence of substantially altered gross fluxes and land carbon pools.

The generally reduced foliar area directly leads to a reduced gross primary production (GPP) of the terrestrial biosphere. The changes to the photosynthetic capacity ( $f_{photo}$ ) (Table 2) often further reduce the uptake, a factor which is most pronounced for crop and tropical evergreen PFTs (Table 6 and Table 2). The GPP reduction is strongest for

the CO2alone experiment and weakest (but still very pronounced) for FAPARalone. Even though the globally integrated posterior GPP values were somewhat different, the relative latitudinal patterns were fairly similar to each other (Fig. 6), and the reduction occurred in all regions, predominantly in tropical forests and grass/crop dominated temperate and boreal zones (Table 2).

Since the net carbon fluxes in the FAPARalone experiment were not constrained by the atmospheric CO<sub>2</sub> observations, the assimilation did not adjust the ecosystem respiration to balance the reduced productivity. This mismatch leads to the overestimation of the growth rate of atmospheric CO<sub>2</sub>. On the time scales of 5 years involved in this study, the respiration was not as much reduced as GPP by the adjustments and as a consequence the net flux to the atmosphere increased. Application of the CO<sub>2</sub> constraint forces the respiration to be reduced as well to match the atmospheric sig-

for what time period 2005-2009?

in all simulations i.e. CO2alone, FAPARalone & JOINT?

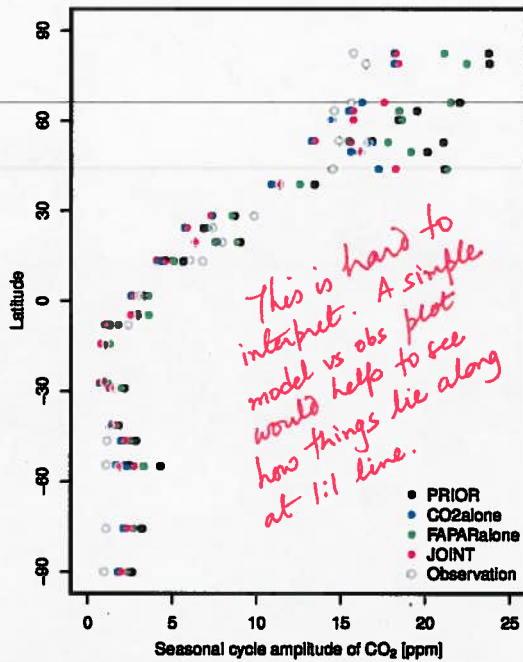


Figure 5. Latitudinal distribution of atmospheric CO<sub>2</sub> seasonal cycle amplitude, calculated as the difference between the maximum and minimum CO<sub>2</sub> mole fraction of the averaged seasonal cycle of the linearly de-trended signal from 2005 - 2009.

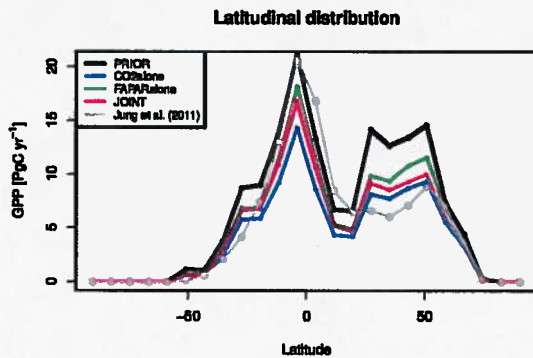


Figure 6. Latitudinal distribution of GPP for the prior and posterior models and comparison with the estimates of Jung et al. (2011).

nal. Since JSBACH models autotrophic respiration as a function of GPP (Eq. 18), which thus equilibrates quickly to any changes in GPP, the reduction in heterotrophic respiration is mainly driven by a reduction of the initial soil carbon pool to 50% and 51% for the JOINT and CO<sub>2</sub>alone experiment, respectively (Table 6).

How does this reduction happens so quickly given the slow time scales associated with the soil carbon pool?

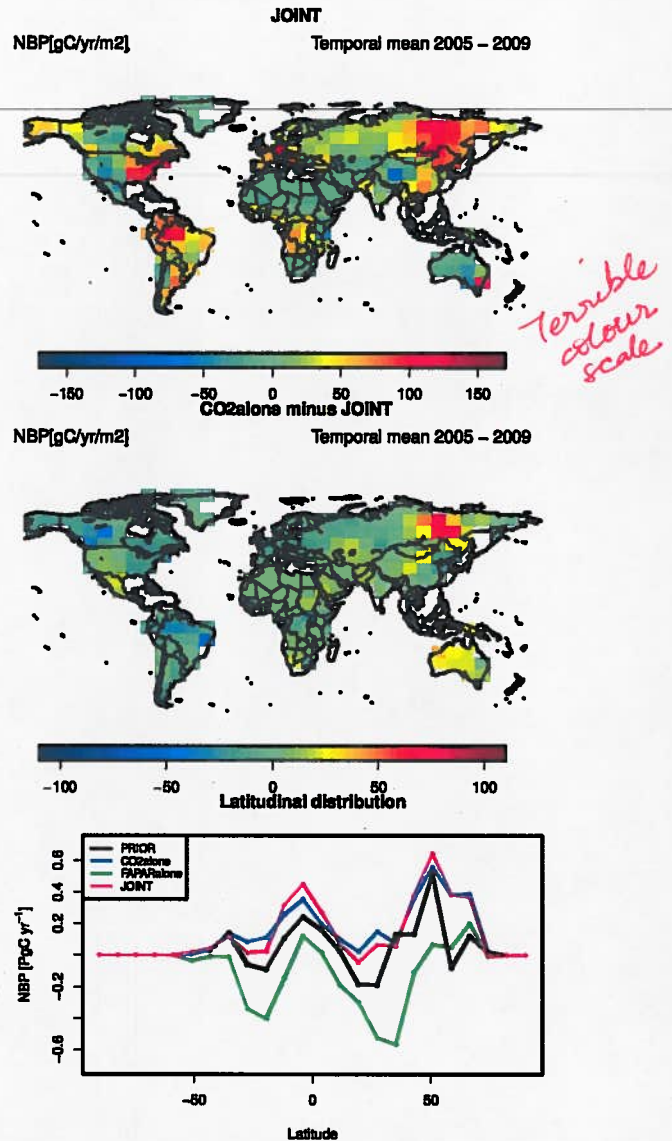


Figure 7. Temporally averaged NBP of the JOINT assimilation, differences of CO<sub>2</sub>alone to the JOINT experiment and the latitudinal distribution for the prior and posterior models.

Despite the similarity of the global NBP for the experiments with CO<sub>2</sub> as a constraint, the spatial patterns of the NBP are different between the CO<sub>2</sub>alone and JOINT experiments (Fig. 7). The net uptake in both experiments originates from boreal and tropical regions. While the JOINT experiment shows an uptake in the boreal regions of coniferous evergreen and coniferous deciduous dominated pixels, the



14

CO2alone uptake is even more concentrated to the coniferous deciduous regions. These differences will be further discussed in Sect. 4.4.2.

#### 4.4 Regional differences among the experiments

5 In the following we focus on differences in the spatial patterns of the results obtained for tropical regions and the boreal zone to highlight the interplay between parameters in a global, multi-data stream application of the MPI-CCDAS either by compensating effects between different model processes within one PFT as occurring in the tropics (Sect. 4.4.1) or by compensations between different parts of the globe (Sect. 4.4.2).

##### 4.4.1 Tropics

15 The modelled foliar area in the tropics (mainly the tropical evergreen tree PFT) was similar for the JOINT and FAPARalone experiments (Fig. 3), but smaller for CO2alone. Notwithstanding the difference in foliar area, the net land-atmosphere CO<sub>2</sub> exchange (Fig. 7) of the JOINT experiment was closer to the posterior estimate of CO2alone than to that of FAPARalone in terms of absolute values. GPP (Fig. 6) lies between the two single data stream experiments, being closer to FAPARalone. This result was caused by compensating effects of the different observational constraints (Fig. 8 and Table 2): the phenological parameters, notably  $\tau_w$  and  $\Lambda_{max}$ , were substantially different between the FAPARalone and JOINT experiment, yet their modelled foliar area was very similar (Fig. 3). The reason for this was that the photosynthesis parameter modifier  $f_{photo}$  was reduced strongly in the JOINT experiment, which also drives the smaller GPP (relative to FAPARalone). A consequence of this large reduction in modelled photosynthesis per unit foliar area and ecosystem level GPP was a strong decrease in the potential transpiration rate ( $E_{pot}$ ; Eq. 6) through the effect of net photosynthesis on canopy conductance (Eq. 15). Together with the increase of  $\tau_w$  (Eq. 6) in the JOINT experiment, the decline in  $E_{pot}$  had the same effect on the simulated phenology as the smaller parameter changes in the FAPARalone experiment. The lack of a FAPAR constraint in the CO2alone experiment allowed the assimilation to overly reduce the foliar area by increasing  $\tau_w$  at the prior rate of photosynthesis and thus  $E_{pot}$  to satisfy the constraint by the atmospheric CO<sub>2</sub> observations. As a consequence, due to the water-cycle feedback, the modelled foliar area was clearly different between the JOINT and CO2alone experiments.

##### 4.4.2 Boreal zones

45 The CO2alone and JOINT experiments showed similar global statistics when compared with atmospheric CO<sub>2</sub> observations (Table 5 and Fig. 4). Their global and hemispheric net uptake was similar (Northern Hemisphere: 2.24/2.20 PgC yr<sup>-1</sup>; Southern Hemisphere: 0.98/0.98 PgC yr<sup>-1</sup>), but

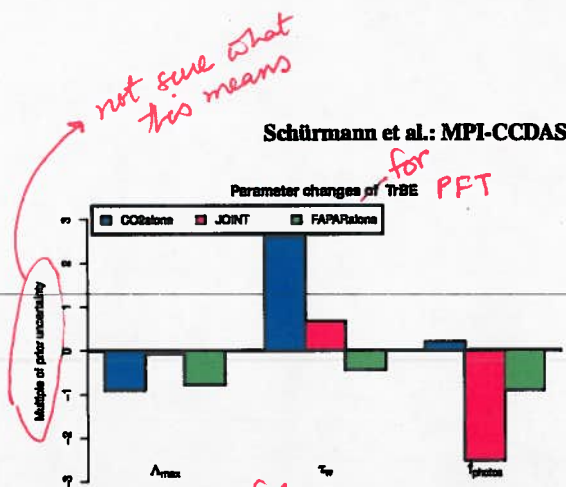


Figure 8. Parameter changes of tropical evergreen trees in multiples of the prior uncertainty.

their underlying spatial patterns were different, in particular in the boreal zone (Fig. 7). The entire boreal zone took up a large share of the global carbon sequestration in the JOINT experiment (0.88 PgC yr<sup>-1</sup>), especially in coniferous deciduous (CD) dominated regions of Eastern Siberia (0.30 PgC yr<sup>-1</sup>). The CO2alone experiment showed a similar net C uptake in the boreal region, but the uptake in the CD dominated region was 0.16 PgC yr<sup>-1</sup> stronger than in the JOINT experiment. This difference was mainly driven by larger foliar area and increased leaf-level productivity (parameter  $f_{photo}$ ) of the CD PFT in the CO2alone experiment. In the same latitudinal band, coniferous evergreen trees showed reduced foliar area in the CO2alone experiment compared to the JOINT experiment, reducing the net uptake by 0.16 PgC yr<sup>-1</sup>, such that the differences in these regions cancel each other. These spatial differences can nevertheless be seen as minor differences in the ability of the posterior JOINT and CO2alone experiment in capturing the amplitude of the seasonal cycle at individual northern-most stations.

*I don't think it is okay to neglect these as minor.*

## 5 Discussion

### 5.1 Comparison of the simulated C cycle with independent estimates

75 The application of the CCDAS led to significant changes of the modelled carbon cycle in JSBACH. The average global GPP of the JOINT experiment (111 PgC yr<sup>-1</sup>) was substantially reduced from the prior run (152 PgC yr<sup>-1</sup>) and was slightly lower than independent, data-driven estimates of 119 ± 6 PgC yr<sup>-1</sup> (Jung et al., 2011) and 123 ± 8 PgC yr<sup>-1</sup> (Beer et al., 2010), as well as estimates of comparable land surface models (ranging from 111 - 151 PgC yr<sup>-1</sup>; Piao et al. 2013). Partly driven by the reduction of GPP, the net primary production (NPP) was also significantly reduced (from 66 PgC yr<sup>-1</sup> (prior) to 46 PgC yr<sup>-1</sup> (JOINT)). While this is lower than the commonly accepted reference value of 60 PgC yr<sup>-1</sup>, it is still compatible with the range of available



estimates for NPP of 44 - 66 PgC yr<sup>-1</sup> (Cramer et al., 1999; Saugier and Roy, 2001). The latitudinal distribution of GPP in comparison to an empirical estimate based on satellite data and field measurements (Jung et al., 2011) shows that the reduction of GPP occurred across the globe, leading to a better agreement of GPP in the Northern extra-tropics between 30°N and 60°N, but a smaller simulated GPP in the tropical rain forests (Fig. 6). The reduction of GPP in the Northern extra-tropics is likely associated with the overestimation of the seasonal cycle of atmospheric CO<sub>2</sub> by the prior model, which was successfully reduced primarily by reducing Northern extra-tropical productivity, in particular in temperate and boreal grasslands.

Despite the strong reduction in NPP, the posterior models stored only little less C in vegetation (389 - 420 PgC) than the prior model (424 PgC). All of these estimates are lower than the 556 PgC vegetation carbon based on updated Olson's major world ecosystem carbon stocks<sup>2</sup>, but comparable to a more recent estimate of global vegetation carbon storage of 442 ± 146 PgC (Carvalhais et al., 2014). The posterior amount of soil carbon from the assimilation runs using atmospheric CO<sub>2</sub> as a constraint compare favourably (within the uncertainty) to the estimates of 1343 PgC based on the Harmonized World Soil Database (HWSD)<sup>3</sup>. This estimate is more appropriate for the presented comparison than the more recent and higher estimate of soil carbon by Carvalhais et al. (2014) of 1836 - 3257 PgC (95% confidence interval), as the latter includes estimates of permafrost carbon, which is not modelled with the current version of the MPI-CCDAS.

The above changes in the carbon cycle led to significant differences in the simulated annual net land carbon fluxes between the assimilation experiments. The assimilation experiments using atmospheric CO<sub>2</sub> as a constraint considerably increased the net land carbon uptake from 1.0 PgC in the prior run to 3.2 PgC during 2005-2009. This increase primarily occurred by reducing ecosystem respiration more than reducing GPP. Our estimate of the net land carbon sink is slightly larger than the residual land carbon sink estimate inferred from atmospheric measurements and auxiliary fluxes by Le Quééré et al. (2015), who derived 2.4 ± 0.8 PgC yr<sup>-1</sup> for the period 2000 - 2009 (even though correcting for pre-industrial carbon fluxes from land to the ocean via rivers would lead to 2.85 PgC yr<sup>-1</sup>; see Le Quééré et al. 2015 and Jacobson et al. 2007). Apart from interannual variability which may have contributed to the differences between the two studies, it is likely that our slightly larger estimate arises from the comparatively small net ocean carbon flux of 1.1 PgC yr<sup>-1</sup> (Rödenbeck et al., 2013), which we prescribed in our assimilation, compared to the estimate of 2.4

± 0.5 PgC yr<sup>-1</sup> of Le Quééré et al. (2015)<sup>4</sup> (which reduces to 1.95 PgC yr<sup>-1</sup> when correcting for the river input). Bearing in mind that the atmospheric CO<sub>2</sub> observations more directly constrain the net land carbon fluxes at seasonal and annual scales than the gross fluxes or carbon pools, assuming a larger ocean net carbon flux would have reduced the land uptake to be more compatible with the estimate of Le Quééré et al. (2015).

## 5.2 Comparison to previous studies

Our results are consistent with earlier studies using JSBACH (Dalmonech and Zaehle, 2013) showing that JSBACH overestimates the seasonal cycle amplitude of atmospheric CO<sub>2</sub>. The posterior estimates of this amplitude was considerably reduced and hence improved in all three experiments (Fig. 5). This also holds for FAPARalone, for which the comparison with CO<sub>2</sub> is an independent evaluation. Note that the prior we reported here already relies on a corrected maximum leaf area index ( $\Lambda_{max}$ ) of coniferous evergreen trees (see Sect. 3). For the run with the off-the-shelf configuration of JSBACH (results not shown), the high latitude mean seasonal cycle amplitude was clustered around 30 ppm which means an overestimation of about 15 ppm. In the prior reported here, this overestimation reduced to about 5 - 10 ppm and further reduced in the FAPAR alone experiment (Fig. 5). Given this information, boreal phenology considerably controls the seasonal cycle of the high latitude atmospheric CO<sub>2</sub>-signal and TIP-FAPAR can improve this aspect even though the CO<sub>2</sub> trend is deteriorated (Fig. 4). Obviously, adding CO<sub>2</sub> as a constraint further improves the fit to the seasonal cycle amplitude. *conclusion*

This is also supported by Kaminski et al. (2012) who assimilated CO<sub>2</sub> and a different FAPAR product (Gobron et al., 2007) jointly, using the BETHY-CCDAS. They found an improved seasonal cycle amplitude of CO<sub>2</sub> for their joint assimilation with real data, which is in line with our findings. Through factorial uncertainty propagation with their assimilation scheme (Mission benefit analysis), Kaminski et al. (2012) also found that the inclusion of FAPAR yields only a moderate uncertainty reduction in the simulated carbon fluxes and mainly reduces the water flux uncertainties. This indicates that FAPAR only added little information to the modelled carbon cycle in addition to atmospheric CO<sub>2</sub>. We in contrast have shown a considerable impact of TIP-FAPAR by altering the spatial net C flux patterns between the JOINT and CO2alone experiments.

Our study also showed a considerable difference of GPP estimates that are not likewise reflected in the net carbon fluxes, as these are more directly constrained by CO<sub>2</sub>. Also Koffi et al. (2012), using a variant of the BETHY-CCDAS (Rayner et al., 2005; Scholze et al., 2007), found large dif-

<sup>4</sup>The estimates of Rödenbeck et al. (2013) and Le Quééré et al. (2015) are not fully compatible because they differ in the accounting of carbon fluxes from rivers to the ocean.

<sup>2</sup><http://cdiac.ornl.gov/epubs/ndp/ndp017/ndp017b.html>

<sup>3</sup><http://webarchive.iiasa.ac.at/Research/LUC/External-World-soil-database/HTML/>

Is this 2D dataset? I would presume so.



ferences in their posterior GPP-estimates ranging from 109 - 164 PgC yr<sup>-1</sup> when using different transport models, atmospheric station densities and prior uncertainties. As in our study, their relatively large GPP-ranges are not reflected in the net fluxes, as these are more directly constrained by the atmospheric CO<sub>2</sub> network. A striking difference to the results of Koffi et al. (2012) occurs in the tropics, where they overestimate GPP compared to data-driven estimates, whereas the MPI-CCDAS underestimates GPP. As will be discussed later (Sect. 5.3.2), our underestimation of tropical GPP is likely a compensating effect arising from the respiration part of the model that only can be modified globally. This is not the case for the BETHY-CCDAS, which allows for a spatially more explicit control on heterotrophic respiration. It appears thus likely that a larger posterior GPP in the MPI-CCDAS could be expected with a system allowing for more spatial freedom in the respiration part of the assimilation system, for instance by making  $f_{\text{aut\_leaf}}$  and  $f_{\text{slow}}$  vary by plant functional type. Regardless of this difference, our work further supports earlier findings (Rayner et al., 2005; Scholze et al., 2007; Koffi et al., 2012) that despite some constraint on Northern extra-tropical GPP, the global land GPP cannot be well constrained with atmospheric CO<sub>2</sub> alone. It appears thus vital that additional information is provided, especially in tropical regions, to further reduce uncertainty in the spatial distribution of the gross fluxes. This likely will propagate to an improved estimate of the net CO<sub>2</sub>-fluxes as well.

Within the BETHY-CCDAS, Rayner et al. (2005) found a very pronounced decrease of NPP from 68 PgC yr<sup>-1</sup> in the prior run to 40 PgC yr<sup>-1</sup> in the posterior run. This decrease was driven by a decrease of their parameter  $f_{R,\text{leaf}}$  (a value also achieved by Scholze et al., 2007), which is functionally comparable to the MPI-CCDAS parameter  $f_{\text{aut\_leaf}}$ . Their estimate is thus similar to our strong NPP-reduction (JOINT NPP: 46 PgC yr<sup>-1</sup>). This apparent similarity towards relatively small numbers (compared to other estimates) should not mislead to the conclusion that global NPP is well constrained from atmospheric CO<sub>2</sub>, because it ignores spatial offsets between the estimates, and the fact that the MPI-CCDAS and BETHY-CCDAS approaches to estimate NPP from GPP are fairly similar. Assimilation of CO<sub>2</sub> into other, simpler biosphere models achieved ranges for NPP from 36 to 53 PgC yr<sup>-1</sup> given different model formulations (Kaminski et al., 2002).

### 5.3 Critical appraisal of the current MPI-CCDAS

With the set-up of the cost function and given the tangent-linear version of the JSBACH model, the assimilation problem for the MPI-CCDAS is clearly defined and solutions of the problem are by construction compatible with the model dynamics. This is a considerable difference to alternative methods, but also means that in the posterior estimates, any model structural deficits will be compensated for by unrealistic parameter values or can be detected in large model-data

residuals. This allows to detect model structural errors and/or deficits in the set-up, which then can lead to a reformulation of the forward model (see e.g.: Kaminski et al., 2003; Rayner et al., 2005; Williams et al., 2009; Kaminski et al., 2013). The MPI-CCDAS framework described here can be steadily improved through regular improvements of the JSBACH model structure by including missing or correcting false model parametrisations (e.g. Knauer et al., 2015). The system is versatile enough to add more constraints from relevant and complementary, multiple data sources (Luo et al., 2012) to come up with more robust regional estimates than the current atmospheric inversion allow.

### 5.3.1 Assimilation procedure

The results clearly show that two data-streams can be successfully integrated with the MPI-CCDAS. The posterior parameter values (Table 2) were different between the FAPARalone and JOINT as well as the CO<sub>2</sub>alone and JOINT experiments, showing that the joint use of the two data streams added information to the posterior result by preventing the degradation of the phenology simulation when trying to fit the CO<sub>2</sub> observations (Table 5 and 4). Hence, even though the JSBACH phenology is only weakly influenced by the carbon cycle and mainly controlled by other drives (e.g.: soil moisture, temperature), there are strong interactions among carbon and water cycle parameters and simulated FAPAR, a finding supported by Forkel et al. (2014). Thus the combination of different data streams in the JOINT experiment helped estimating parameters of different processes to remain within acceptable bounds. The capability of assimilating multiple data streams simultaneously is a distinct advantage of the MPI-CCDAS over alternative strategies that assimilate multiple data streams by following a sequential design of assimilating FAPAR prior to carbon cycle information. Such an algorithm would break the model linkage between phenological and photosynthesis parameters, which would lead to situations where the observations will not be equally well matched as in a joint assimilation. Since our results have demonstrated that a joint assimilation is feasible without impairing the fit to the individual data sources, a joint assimilation approach appears therefore recommendable.

While the assimilation procedure achieved a strong reduction of the cost function and the norm of the gradient (see Table 3), the norm of the gradient was closest to zero in the case of the FAPAR constraint, but not for CO<sub>2</sub>, even though the relative reduction in the CO<sub>2</sub>-cases was larger. Such a non-zero gradient was also noted by Rayner et al. (2005) in their CO<sub>2</sub> assimilation with the BETHY-CCDAS. The fact that the MPI-CCDAS successfully reduces the norm of the gradient for FAPAR suggests that this is not a general failure of the MPI-CCDAS, but specific to the particularities of the CO<sub>2</sub> set-up. It is presently unclear, what is causing the assimilation to fail to reach the minimum of the cost function, and

→ reword  
this. I  
think, you  
mean weakly  
controlled  
by  
atmospheric  
CO<sub>2</sub> concentration  
atmos. CO<sub>2</sub>



further tests with alternative station network settings, parameter priors or time-periods are needed to evaluate the cause. We believe that our results can still be meaningfully interpreted and used to evaluate the general capacity of the MPI-CCDAS as a comprehensive data assimilation tool.

### 5.3.2 Parameter set-up

Another cautionary note about the posterior parameter values is warranted: Some of the parameters of the JOINT and CO2alone experiment were altered strongly compared to the assumed prior uncertainty. This is possible within the MPI-CCDAS, because the prior contribution to the cost-function is weak due to the small number of parameters compared to the number of observations. One example is the  $f_{slow}$  parameter, which controls for the initial soil C pool size and thus the disequilibrium between GPP and respiration (Table 2). Another example is the photosynthesis parameter  $f_{photos}$  for the tropical evergreen PFT in the JOINT experiment, which was reduced by more than 2.5 times the prior uncertainty and to roughly 75% of its prior value. As a consequence, the assimilation procedure can result in parameter values with small prior probabilities. This either points toward too tight prior uncertainties or to model structural problems. The current MPI-CCDAS excludes the model spin-up from the assimilation procedure which likely leads to such structural problems as discussed in the following.

The solution applied here for the spin-up was to allow the MPI-CCDAS to manipulate the initial soil C pool by one globally valid modifier. Our results demonstrate that using this approach it is possible to reproduce very well the space-time structure of the atmospheric CO<sub>2</sub> budget at the time scale of several years (Fig. 4 and Table 5). However, this approach introduces an undesirable imprint of the spatial distribution of the prior productivity on the final model outcome, which may cause imperfections in the ability of the MPI-CCDAS to accurately capture the spatial distribution of the net land carbon uptake. Allowing for more spatially explicit modifiers for the initial carbon pools (as is done in the BETHY-CCDAS) by e.g. linking the initial soil disequilibrium to a particular PFT, would be a first step forward.

The stiffness of the MPI-CCDAS respiration parametrisation likely also caused the reduction of temperate GPP to propagate into the tropical zone, leading to the strong change of  $f_{photos}$  for the tropical evergreen PFT in the JOINT experiment. Because the overall net CO<sub>2</sub> flux is constrained by the atmospheric observations, reduction in temperate GPP requires a corresponding adjustment of the ecosystem respiration to balance the budget. While lowering GPP also reduces autotrophic respiration (Eq. 18), any further reduction in respiration in the temperate zone by adjusting autotrophic ( $f_{aut\_leaf}$ ) or heterotrophic respiration parameters ( $Q_{10}$ ,  $f_{slow}$ ) would also affect tropical respiration, because in the current version of the MPI-CCDAS these parameters are assumed to be valid globally. To balance the budget, a re-

duction in tropical GPP might have been required. Because of enough water availability in the tropics a phase-shift in the dry-wet cycle in the Amazonian rain forest may play a minor role in the down-regulation of GPP during the assimilation. At least no phase mismatch in atmospheric CO<sub>2</sub> is observed at Mauna Loa (Fig. 4) that would suggest such a problem.

We also found that extreme parameter changes in vegetation production to better match the observational constraints would impede finding an optimum solution with realistic parameter values. A first series of experiments with the standard maximum foliar area for the coniferous evergreen PFT (not reported here) revealed a bias of 0.4 in FAPAR in the boreal zone. While, in these experiments, the FAPARalone assimilation successfully removed this bias, the lack of a re-calculated initial carbon pool meant that the spatial patterns of the initial carbon pools belonging to the high-biased FAPAR values caused compensating effects in the carbon fluxes of other PFTs in the JOINT assimilation run. To avoid this significant bias from affecting our results, the MPI-CCDAS experiments reported here are therefore based on a reduced prior estimate for the coniferous evergreen PFT to account for the sparseness of boreal forests. Strictly speaking this is a violation of the Bayesian theory and a double counting of the information contained in the FAPAR observations. We nevertheless think that this violation is appropriate, as it corrects for a known model shortcoming and since we do not change the prior uncertainties and do not evaluate the posterior probabilities of the parameters.

### 5.4 Outlook

Beside the previously discussed limitation related to the spin-up and the representation of initial carbon pools, we can suggest also other analysis and system developments to further improve the MPI-CCDAS.

The discrepancies between FAPARalone and JOINT in the foliar area estimates for crop-dominated regions, even though large in extent, originates from the exclusion of TIP-FAPAR as constraint for these regions. This likewise affected the extra-tropical deciduous PFT, that co-occurred dominantly in the same pixels. Increasing the constraining power of TIP-FAPAR by either adding more pixels as constraints or by increasing the resolution to finer grids might further improve the phenology. We also did not analyse the phenological model behaviour in full detail, because the focus of this work lied on analysing the benefit of the joint assimilation. More focusing on only the FAPAR assimilation also in a spatially more explicit manner could further evaluate the phenology scheme and improve the modelled foliar area.

We have demonstrated that the JSBACH model is capable of reproducing the seasonal cycle and 5 year trend of the observed atmospheric CO<sub>2</sub> (Fig.s 4 and 5 and Table 5). We have applied a careful selection of stations to avoid the impact of local sources on modelled atmospheric CO<sub>2</sub> mole fractions, which cannot be simulated with the current coarse

reword this to say more explicitly what you mean

unclear

What does this mean?



resolution of the MPI-CCDAS. Nevertheless, the evaluation with the cross-validation sites demonstrates a good skill of the posterior model also for these sites, suggesting that the observed CO<sub>2</sub> dynamics at monthly to yearly time scales are reasonably well captured. Our study supports earlier findings that despite some constraint on Northern extra-tropic production, the constraint of observed atmospheric CO<sub>2</sub> on global production is small (Koffi et al., 2012). It further also supports the studies of Rayner et al. (1999), Kaminaki et al. (1999) and Peylin et al. (2013) that the observational network of atmospheric CO<sub>2</sub> only constrains a limited spatial resolution. But we also demonstrated the value of using a CCDAS instead of a pure atmospheric inversion to estimate land fluxes, because it can ingest other data streams, which might further constrain the regional estimates. In this first version of the MPI-CCDAS we have assumed the net fluxes other than those simulated with JSBACH (fossil fuel emissions and ocean exchange), as well as the atmospheric drivers to JSBACH to be perfectly known, and thus impute all the model-data mismatch on shortcomings of the land-surface model. It would be desirable to also account for the uncertainties in these components of the modelling system to more robustly identify potential model shortcomings.

Our results show that applying FAPAR and atmospheric CO<sub>2</sub> as a constraint for the JSBACH model leads to an improved simulation of phenology and Northern extra-tropic GPP. As a consequence of the assimilation procedure, the model also captures the magnitude of the global and hemispheric net biome exchange. This is a major step forward to including better constrained terrestrial models for the estimation of the global carbon budget (Le Quéré et al., 2015). However, we set-up the model such that it attributes the difference between prior and posterior sink (i.e. 2.2 PgCyr<sup>-1</sup>) to the soil carbon storage. But it has been long known that the terrestrial net carbon uptake, and thus the CO<sub>2</sub> signal seen by the atmospheric observations, is strongly affected by natural (such as fire) and anthropogenic disturbances (such as land-use change; Houghton et al. 2012). These processes contribute to the disequilibrium of vegetation and soil carbon pools with vegetation production, and thus affect the spatial pattern of terrestrial carbon release and uptake. Without consideration of these processes, one should be careful in analysing the MPI-CCDAS projected carbon cycle trends and attribution of drivers of the trends. The tangent-linear version of the JSBACH model contained in the MPI-CCDAS already has the appropriate modules to simulate disturbance by fire (Lasslop et al., 2014) and land-use (Reick et al., 2013). A further development of the MPI-CCDAS could be to activate these processes. In order to improve on the current situation it might also be desirable to constrain the post-disturbance dynamics of the carbon pools or at least to analyse how well these are constrained. This would also allow to add more data streams to potentially disentangle the tight parameter linkages in the model.

## 6 Conclusions

The assimilation of five years of remotely sensed FAPAR and atmospheric CO<sub>2</sub> observations with the MPI-CCDAS was generally successful in that the fairly substantial model-data mismatch of the prior model was largely reduced. The assimilation procedure strongly reduced the too large prior-estimate of GPP, and generally led to an improvement of the simulated carbon cycle and its seasonality. The resultant carbon cycle estimates compared favourably to independent data-driven estimates, although tropical productivity was lower than these estimates. The posterior global net land-atmosphere flux was well constrained and commensurate with independent estimates of the global carbon budget. Our analysis of the prognostic fluxes for a consecutive 2-year period as well as at stations withheld from the assimilation procedure demonstrates that our results are robust.

The factorial inclusion of FAPAR and atmospheric CO<sub>2</sub> as a constraint clearly demonstrated that the two data streams can be simultaneously integrated with the MPI-CCDAS. We have shown the potential of multi-datastream assimilation by adding TIP-FAPAR as a constraint and have shown how this data streams helps constraining the foliar area without degrading the ability of the model to capture seasonal and yearly dynamics of the atmospheric CO<sub>2</sub> mole fractions. However, the multi-data assimilation also pointed to model structural problems in the initialisation, which need to be addressed. Nevertheless, our study highlights the potential of adding new data streams to constrain different processes in a global ecosystem model.

This study thus provides an important step forward in the development of global atmospheric inversion schemes, by adding a process-based component to disentangle drivers of the terrestrial carbon balance, and the opportunity to apply multiple data streams to constrain them in the framework of a land surface model belonging to a coupled carbon-cycle climate model. On the one hand improving the assimilation system and on the other hand adding more data streams can ultimately lead to regionally constrained estimates of the terrestrial carbon balance for the assessment of current and future trends.

## Code availability

The JSBACH model code is available upon request to S. Zaehle (soenke.zaehle@bgc-jena.mpg.de)

The TM3 model code is available upon request to C. Rödenbeck (christian.roedenbeck@bgc-jena.mpg.de)

The TAF generated derivative code is subject to license restrictions and not available.

unclear

68

80

88

70

78

86

84

92

100

98

100



Schürmann et al.: MPI-CCDAS

19

Appendix A: CO<sub>2</sub> station list

The stations of atmospheric CO<sub>2</sub>-observations used for assimilation and evaluation are given in Table A1 resp. Table A2.

Table A1. CO<sub>2</sub> stations used in the assimilation together with their median uncertainty. *what does this mean?*

ID	Longitude	Latitude	Median Uncertainty
MNM	153.97	24.30	1.4
SBL	-60.02	43.93	5.9
ALT	-62.52	82.45	1.8
ASC	-14.42	-7.92	1.1
AZR	-27.19	38.76	1.9
BHD	174.90	-41.40	1.0
CHR	-157.17	1.70	1.0
CRZ	51.85	-46.45	1.0
EIC	-109.45	-27.15	1.1
ESP	-126.83	49.56	2.9
GMI	144.78	13.43	1.2
HBA	-26.65	-75.58	1.0
ICE	-20.21	63.30	1.9
KER	-177.15	-29.03	1.0
KUM	-154.82	19.52	1.6
MHD	-9.90	53.33	2.4
MID	-177.37	28.22	1.7
MQA	158.97	-54.48	1.0
RPB	-59.43	13.17	1.1
SEY	55.17	-4.67	1.0
SHM	174.10	52.72	2.1
SIS	-1.23	60.23	3.1
STM	2.00	66.00	3.2
TDF	-68.48	-54.87	1.0
ZEP	11.88	78.90	2.3
MLO	-155.58	19.53	1.1
SMO	-170.57	-14.25	1.0
SPO	-24.80	-89.98	1.0

Table A2. CO<sub>2</sub> stations used for evaluation that have not been used as constraints for the assimilation.

ID	Longitude	Latitude
PAL	24.12	67.97
PRS	7.70	45.93
RYO	141.83	39.03
YON	123.02	24.47
CBA	-162.72	55.20
CFA	147.06	-19.28
CGO	144.70	-40.68
COI	145.50	43.15
CYA	110.52	-66.28
HAT	123.80	24.05
IZO	-16.48	28.30
KEY	-80.20	25.67
LEF	-90.27	45.93
LJO	-117.25	32.87
LMP	12.61	35.51
MAA	62.87	-67.62
NWR	-105.60	40.05
PSA	-64.00	-64.92
SUM	-38.47	72.57
TAP	126.13	36.73
UTA	-113.72	39.90
UUM	111.10	44.45
WIS	34.88	31.13
WLG	100.91	36.28
BRW	-156.60	71.32
SYO	39.58	-69.00
CMN	10.70	44.18
SCH	7.92	47.92

Appendix B: Mapping variants

For performance reasons, the assimilation is not performed in the physical parameter space but parameters  $p$  are transformed to  $x$  expressed in multiples of the prior uncertainty, the intrinsic units of the problem (Kaminski et al., 1999). The most basic mapping is:

$$x = \frac{p - p_0}{\sigma_{\text{prior}}} \Leftrightarrow p = p_0 + \sigma_{\text{prior}} * x \quad (\text{B1})$$

An extension of this is to apply lower bounds in the mapping back to physical space with

$$p = p_{\text{min}} + x_{\text{low}} / x * \sigma_{\text{prior}}$$

only if

$$x < x_{\text{low}} = \frac{p_{\text{min}} + \sigma_{\text{prior}} - p_0}{\sigma_{\text{prior}}} \quad (\text{B2})$$

with  $p_{\text{min}}$  the minimum allowed parameter value.

Appendix C: Parameter values

Some parameters were modified with a factor within the MPI-CCDAS, because model structure did not allow to directly change these values and thus such an approach was required. The parameter values are listed in Table C1.

Appendix D: PFT-distribution

The vegetation distribution of the PFT's as prescribed in the MPI-CCDAS is given in Fig. D1.



Table C1. Values of those parameters that have been changed with a multiplicative factor during the assimilation.

PFT	TrBE	TrBD	ETD	CE	CD	RS	TeH	TeCr	TrH	TrCr
Prior $\Lambda_{max}$ [ $m^2/m^2$ ]	7.0	7.0	5.0	1.7	5.0	2.0	3.0	4.0	3.0	4.0
Joint $\Lambda_{max}$ [ $m^2/m^2$ ]	6.9	4.1	4.9	1.7	3.2	2.7	1.9	2.5	1.6	2.1
Prior $V_{c,max}$ [ $\mu mol/m^2s$ ]	39.0	31.0	66.0	62.5	39.1	61.7	78.2	100.7	8.0	39.0
Joint $V_{c,max}$ [ $\mu mol/m^2s$ ]	29.2	33.3	65.1	59.2	40.6	62.1	75.4	67.9	8.3	34.1
Prior $J_{max}$ [ $\mu mol/m^2s$ ]	74.1	58.9	125.4	118.8	74.3	117.2	148.6	191.3	140.0	700.0
Joint $J_{max}$ [ $\mu mol/m^2s$ ]	55.5	63.3	123.7	112.5	77.2	117.9	143.2	129.0	145.0	611.2

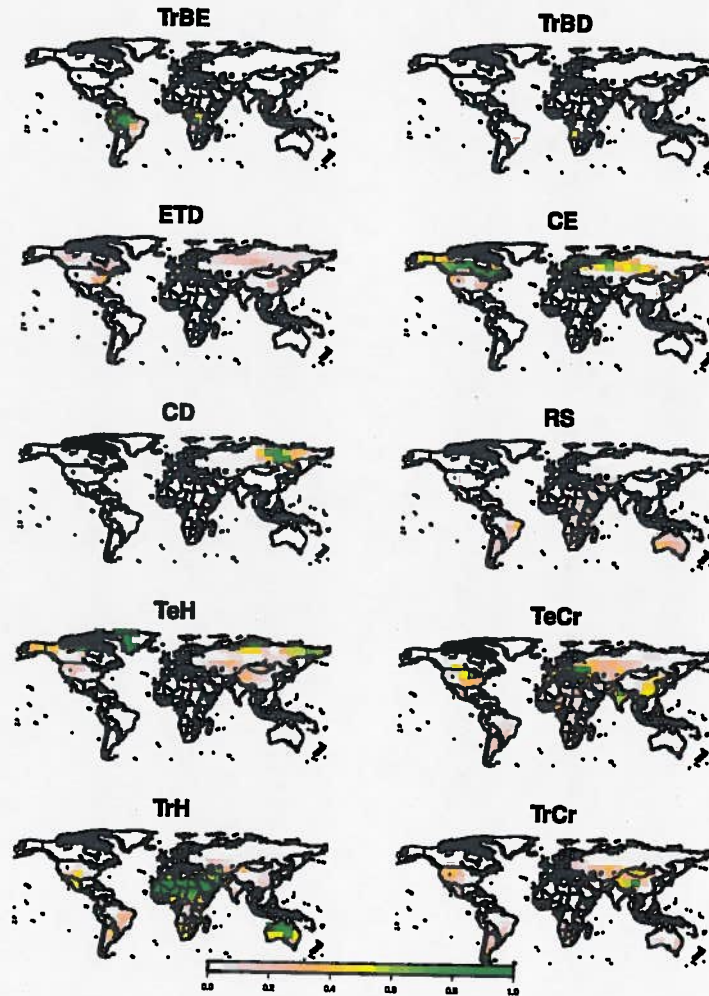


Figure D1. Fractional vegetation coverage of the PFT's as prescribed in the MPI-CCDAS. See Table 1 for abbreviations.